Available online at www.sciencedirect.com
SCIENCE DIRECT®
Journal of Power Sources 152 (2005) 1–15
JOURNAL OF POWER SOURCES
www.elsevier.com/locate/jpowsour

Review

Recent development of non-platinum catalysts for oxygen reduction reaction

Bin Wang *

Departments of Chemistry & Physics and Chemical Engineering, Lamar University, P.O. Box 10022, Beaumont, TX 77710, USA

Received 25 April 2005; accepted 16 May 2005
Available online 18 August 2005

Abstract

The slow oxygen reduction reaction (ORR) kinetics on Pt catalysts is among the most limiting factors in the energy conversion efficiency of the state-of-the-art PEMFC. Also, Pt is scarcely available at a high price. Alternative materials are therefore highly sought for fuel cell applications. This review will concentrate on the electrochemical ORR on non-Pt catalysts, especially the experimental development during the past five years. Emphasis is placed on the understanding of the fundamental materials chemistry. This understanding seems pivotal for new designs of PEM cathode materials. Future outlooks are provided for researchers in engineering to select promising candidates for ORR.

Keywords: PEM fuel cell cathode; Oxygen reduction reaction; Non-platinum based; Nano-scale materials; Molecular-level assembly

Contents

Fuel cell vehicles (FCVs) represent a radical departure from vehicles with conventional internal combustion engines. FCVs can be fueled with pure hydrogen gas or hydrogen-rich fuels, such as methanol, natural gas, or even gasoline. FCVs fueled with pure hydrogen emit no pollutants – only water and heat – while those using hydrogen-rich fuels produce only small amounts of air pollutants. In addition, FCVs can be twice as efficient as similarly sized conventional vehicles and may also incorporate other advanced technologies to increase efficiency [1]. A polymer electrolyte membrane (PEM) fuel cell, shown in Fig. 1, consists of two electrodes and one membrane separating the two electrodes. PEM fuel cells are the most promising type for FCV commercial

* Tel.: +1 409 880 7976; fax: +1 409 880 8270.
E-mail address: wangbx@hal.lamar.edu.

0378-7753/$ – see front matter © 2005 Elsevier B.V. All rights reserved.
doi:10.1016/j.jpowsour.2005.05.098

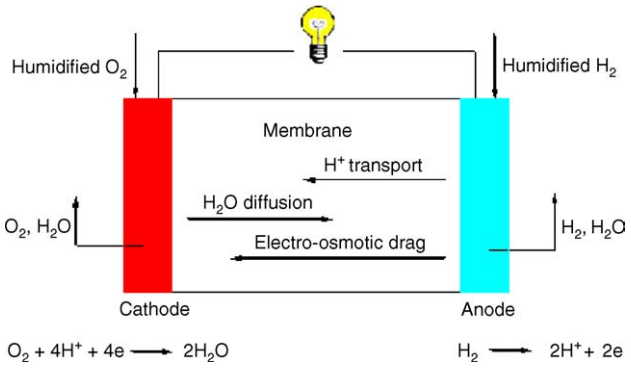

Fig. 1. Simplified PEM fuel cell reactions.

realization because they can be operated at close to ambient temperature range 60–80 °C. As illustrated in Fig. 1, there are two types of electrochemical reactions occurring at the surfaces of the electrodes of a hydrogen PEM fuel cell (PEMFC), oxidation of hydrogen at the anode and reduction of oxygen at the cathode. Platinum-based catalysts are widely used as the anodic electrode material for hydrogen oxidation. The hydrogen oxidation reaction has a lower oxidation overpotential and a higher kinetic rate. On the cathodic side, however, the low reaction rate of the oxygen reduction reaction (ORR) leads to a higher reduction overpotential in the performance condition of PEMFC. The slow ORR kinetics on Pt catalysts is among the most limiting factors in the energy conversion efficiency of the state-of-the-art PEMFC. Also, Pt is scarcely available at a high price. Alternative materials are therefore highly sought for fuel cell applications.

Improved cathode catalysts would have a dramatic impact on the fuel cell efficiency. In this review, we will concentrate on the electrochemical ORR on non-Pt catalysts, especially the experimental development during the past five years from peer-reviewed journal publications. A few examples of ORR in basic aqueous solutions, which would be for alkaline fuel cell applications, or in physiological conditions with biological importance, will be included in hope of modifications on those structures to be made to suit PEMFC. The objective of this work is to provide a present, concise survey in materials development related to ORR, to help researchers in engineering more effectively select concerted candidates for this important fuel cell reaction.

1. ORR catalyzed by noble metal electrodes

Catalytic activities of noble metals toward ORR can be grouped into two general categories, on metal slabs and on metal nanoparticles. We will start discussion the ORR catalyzed by bulk noble metals, followed by nanoparticulate systems. The term noble metals indicate the fifth and sixth period, group 8B elements. These elements are known excellent catalysts for many chemical reactions, yet usually with

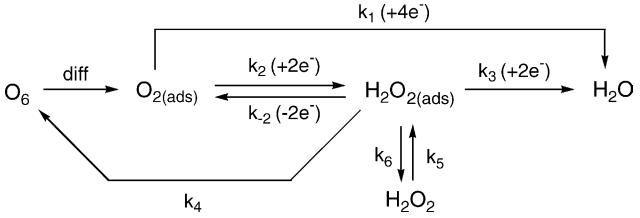

Scheme 1.

high materials cost. Gold and silver are also included in this group simply because of the cost relevance.

1.1. ORR catalyzed on bulk noble metals

ORR process includes several individual reactions (Scheme 1). For electrochemical catalytic ORR analysis, two general processes are examined mostly; each process may contain a few discrete steps. One is production of water through a four-electron pathway, and the other is production of hydrogen peroxide through a two-electron pathway. The desired feature for a successful ORR catalyst would reduce oxygen molecules to water through the four-electron route. Incomplete reduction of oxygen to hydrogen peroxide not only leads to low energy conversion efficiency, but also produces this reactive intermediate that can further convert to harmful free radical species. ORR on ruthenium in alkaline solution has been analyzed through cyclic voltammetry (CV) and rotating ring–disk electrode (RRDE) techniques [2]. The CV experimental data indicate formation of ruthenium oxide during the reverse scan (anodic curves). The ring currents from the RRDE experiment correspond to the oxidation of peroxide; the small values indicate a four-electron ORR process (Fig. 2). However, the study was conducted in alkaline solution, so the results need to be modified for PEMFC purpose. Instead of pure ruthenium metal, a slab of Ru surface was used to support copper as the ORR catalyst [3]. Scanning tunneling microscope (STM) images demonstrate Cu

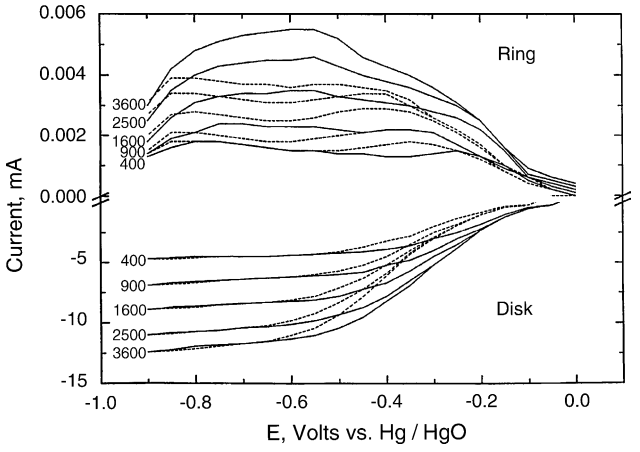

Fig. 2. Rotating ring–disk currents for oxygen reduction on Ru electrode in O_2 saturated 0.1 M KOH at 25 °C. Dotted lines: reverse scan. Solid lines: forward scan (reproduced from [2] by permission of Elsevier).

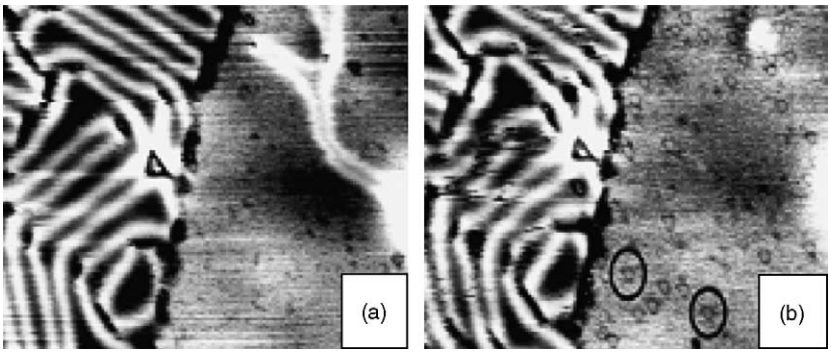

Fig. 3. 50 nm × 30 nm STM images showing the adsorption of O_2 at 300 K on 1 and 2 ML of Cu grown on Ru(0 0 0 1). The exposure is (a) 0.2 L and (b) 5.4 L, respectively. The circles highlight the decoration of the features that appear upon O_2 exposure (reproduced from [3] by permission of Elsevier).

films grown to 1–3 monolayer (ML) thickness on Ru. Oxygen adsorption on the Cu/Ru surfaces is evident from STM images (Fig. 3). Here, ruthenium plays a role to disperse copper films into highly strained phase, which is more reactive toward oxygen dissociation. Using density function theory, it has been predicted that molecular oxygen binds to both Au(1 1 1) and (2 1 1) surfaces [4]. From this study, it also shows that steps and tensile strain facilitate oxygen activation on gold surfaces. Thermal desorption spectrometry (TDS) was used to examine the adsorption/reaction of oxygen on Au(1 1 1) surface [5]. More detailed analysis was provided through collision-induced desportion (CID) experiments [6]. In Fig. 4, the mass 34 signal is evidence of a recombination of $^{16}O_{ads}$ with an impinging $^{18}O_2$ during a plasma-jet exposure. When adlayers of metal are deposited on Au(1 1 1), different ORR behavior of the electrodes has been observed [7]. Au(1 1 1) electrodes modified with 1/3 ML Cu, 1/3 ML Ag, and Bi(2 × 2) all show an almost two-fold increase in reduction current in alkaline solution. A recent study was conducted on using bimetallic catalysts for ORR [8]. The guide of this study is the thermodynamic principles assuming that oxygen molecules dissociate on one metal and oxygen atoms are reduced on the other. The electrocatalytic activities of some binary metal alloys in acidic medium were examined by scanning electrochemical microscopy (SECM). Among the combinations analyzed, Pd/Co on glassy carbon show high ORR activities (Fig. 5). For example, when the substrate potential was at a positive range of 0.7 V, the 90:10 Pd/Co composition showed the highest ORR activity (I-b), about half that of carbon-supported Pt (image not shown), while compositions containing Co more than 20% shows decreased activities. At this substrate potential, pure Pd exhibits no activity. This study provides a method for high throughput design of multi-metallic catalysts.

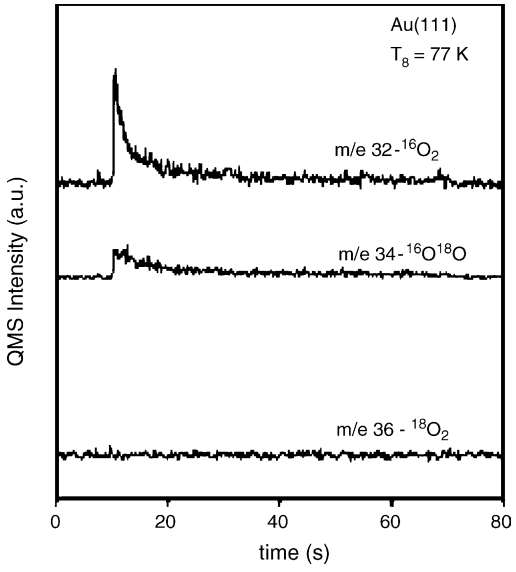

Fig. 4. Desportion measurement at 77 K from Au(1 1 1) following exposure to the $^{18}O_2$ plasma jet, followed by heating to 300 K, then, on cooling back to 77 K, exposure to the $^{16}O_2$ plasma jet (reproduced from [6] by permission of the American Chemical Society).

1.2. ORR catalyzed on nanoparticulate noble metals

During the past two decades, a promising aspect in catalyst development is to employ nanopartiles. Titanium dioxide nanoparticles coated with ML of gold were analyzed in the oxygen desorption experiment [5]. A low-temperature

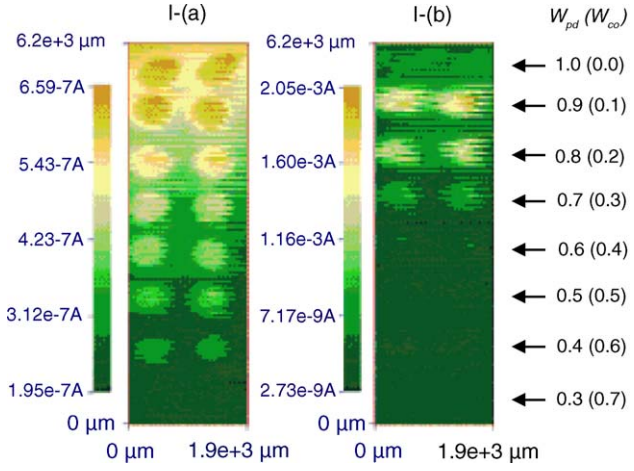

Fig. 5. SECM images of oxygen reduction activity measured on Pd/Co arrays in 0.5 M H_2SO_4, scan rate 0.25 mm s^{-1}, E_S = 0.4 V (I-a), 0.7 V (I-b). W_M is the atomic ratio of metal M (reproduced from [8] by permission of the American Chemical Society).

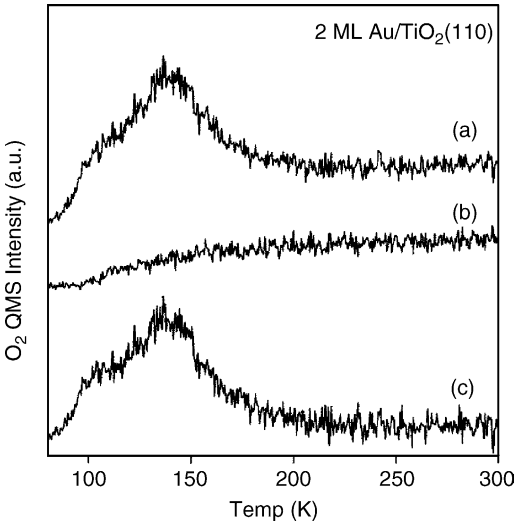

Fig. 6. TDS from a 2 ML Au/TiO_2 sample (a) following exposure to O_2, (b) following exposure to O_2 and then CID and (c) difference between (a) and (b) (reproduced from [5] by permission of the Chemical Society).

desorption feature indicates the presence of molecularly chemisorbed oxygen on a 2 ML Au/TiO_2 surface (Fig. 6). Assuming a first-order desorption, Fig. 6c shows a desorption peak at ∼145 K that corresponds to a binding energy of ca. 0.35 eV. Similarly, the CID experiments demonstrate the presence of $^{16}O^{18}O$ (mass 34) desorption from the Au/TiO_2 surfaces [6]. This fact reveals that molecularly adsorbed oxygen is formed on the surface prior to CID (Fig. 7). In alkaline solution, gold nanoparticles deposited on glassy carbon demonstrate ORR activity [9]. The behavior resembles a four-electron process. Another study analyzed the reaction between gas phase gold clusters with oxygen [10]. Gold clusters (Au_N) with structure $N = 2$, 4 demonstrate low oxygen binding energies, while those with $N = 3$, 5 have high binding energies. Exposure to humidity induces Au_N $-OH^-$, which has the reverse O_2 binding tendency in regard to the bare clusters. The results provide insight into the possible role of water in the activity of gold clusters. Gold clusters were also deposited on boron-doped diamond (BDD) electrode for ORR [11]. Vacuum-deposition followed by annealing affords very stable gold clusters on BDD surfaces. Under acidic conditions, the four-electron ORR pathway was observed for such catalysts. The catalysis is also accompanied with a significant positive shift of the O_2 reduction peak and increase in the current efficiency.

Palladium nanoparticles on gold electrodes were tested for ORR activity [12]. This system can catalyze ORR in KCl solution at −0.2 V through a four-electron pathway; however, the system is not stable. Palladium nanoparticles have also been coated onto carbon nanotubes (CNT) in supercritical carbon dioxide medium [13]. When bare CNT is deposited on a carbon electrode, oxygen reduction occurs at ca. 0.4 V (Fig. 8A). The reduction current increases with the potential decrease, suggesting a kinetics-controlled process. For the Pd–CNT deposited carbon electrode, oxygen reduction shifts to close to 0.5 V (Fig. 8B), and the peak current varies linearly with the square root of the scan rate (figure not shown). This fact indicates that the ORR at Pd–CNT carbon electrode is a diffusion-controlled process. Silver nanoparticles deposited on carbon have also shown the ORR activity in alkaline solution [14]. In comparison to Pt/C system, the onset of the reduction curves at Ag/C only shifts 0.05 V toward negative potential. The ORR at Ag/C seems to be close to a four-electron process. A different nanoparticulate system for ORR in acid solutions is the Cheverel phase $Ru_2Mo_4Se_8$ [15]. The catalyst showed ORR activity of 0.85 mA cm^{-2} under fuel cell operating conditions (0.7 V overpotential), only inferior to Pt by ca. 30%. This catalyst was prepared in a manner involving high temperature (1500 °C) treatment. A modification of preparing similar compounds involved the use of carbonyl complex or carbonaceous ligand in organic solution [16]. The produced carbonaceous ruthenium selenide ($Ru_xSe_yC_vO_w$) nanoparticles were covered by a layer of

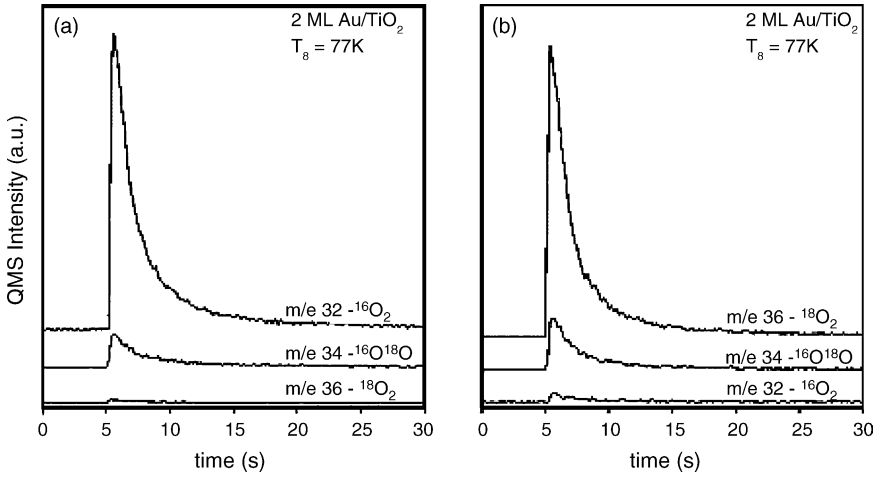

Fig. 7. Kr CID measurement from a 2 ML Au/TiO_2 sample at 77 K of $^{16}O_2$, $^{18}O_2$, and $^{16}O^{18}O$ following: (A) exposure to $^{18}O_2$ plasma at 77 K (i), followed by heating to 300 K and after cooling to 77 K (ii), and exposure to $^{16}O_2$ plasma (iii). In (B), the order of $^{18}O_2$ and $^{16}O_2$ exposures is reversed (reproduced from [6] by permission of the American Chemical Society).

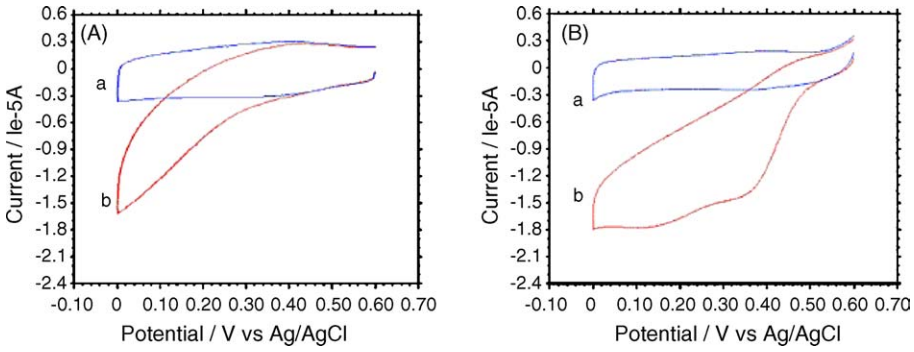

Fig. 8. CV curves obtained at CNT (A) and Pd–CNT (B) on carbon electrodes in 1 M H_2SO_4 saturated with nitrogen (a) and oxygen (b) (reproduced from [13] by permission of Elsevier).

Ru with narrow size distribution ca. 4 nm, determined via transmission electron microscope (TEM) analysis. No ORR results are given in this study. Related to ORR catalytic activities, a study utilizes a matrix of tin oxide and antimony oxide to stabilize RuO_2 for oxygen evolution reaction [17]. At room temperature, such catalysts had a service time of 309 h in a 3 M H_2SO_4 solution under a current density of 0.5 A cm^{-2}.

2. ORR catalyzed by non-noble metal electrodes

The distinction of using non-noble metals is the cost consideration for potential mass products such as FCVs. Most of the metals discussed in this section are transition metals, but some are main group elements. Copper is a widely used catalyst for some important chemical reactions and there is a rich literature of its application in ORR. Komori and coworkers employed STM to study the O_2 adsorption on Cu(0 0 1) surface [18]. Oxygen molecules can adsorb onto and migrate on the Cu surface (Fig. 9). The diffusion barrier of the oxygen adsorbates is smaller at more compressed area, a phenomenon

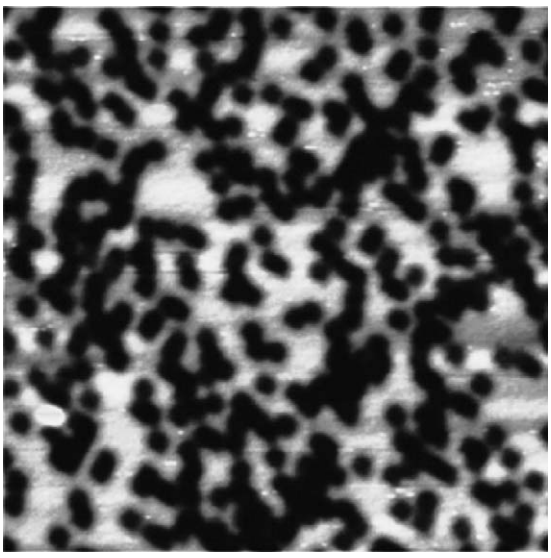

Fig. 9. An STM image showing oxygen adsorption on a clean Cu(0 0 1) (8.5 nm × 8.5 nm) surface (reproduced from [18] by permission of Elsevier).

consistent with the predictions by precursor-mediated dissociative adsorption. The hydrogenation of adsorbed O on Cu(1 1 1) at temperature range 80–600 K was studied with TDS and Auger spectroscopy [19,20]. At temperature above water desorption (150 K), the formation of gaseous water is observed to follow two consecutive step-formation of OH_{ad} then hydrogenated to H_2O_{ad}, which desorbs isothermally (Fig. 10, left). Above 300 K, an apparent acceleration of water formation is observed, a phenomenon attributed to the activation barrier of O_{ad} hydrogenation (Fig. 10, right). A later study found that there is water desorption even at 60 K from such a system, well below the water desorption temperature of 150 K [21]. It was found that the formation of water from OH_{ad} hydrogenation is the rate-determining step with a cross-section of 0.6 $Å^2$. A similar study with Ni(1 0 0) substrate was carried out to examine the ORR under hydrogen exposure at 600 K [22]. Fast formation and desorption of water molecules were observed during the investigations, but no hydroxyl groups were found. Also found is the sequence of oxygen desorption: oxygen atoms desorbs from surface followed by the subsurface oxygen atoms diffuse to the oxygen-depleted surface.

Other than pure metals, metal oxides and alloys have been investigated for their ORR catalytic activities. Titanium dioxide is a known semiconductor that has many interesting catalytic properties. ORR activity was found on anodically formed TiO_2 on Ti surface [23]. From rotating disk electrode (RDE) experiments, it was concluded that the ORR on TiO_2 proceeds through a two-electron process in acidic solutions and four-electron process in basic solutions. Polyoxometallates are a large class of transition metal–oxygen cluster compounds that have unique properties, such as stability, commercial availability and relative ease of synthesis. Some of these compounds have received particular attention as proton conducting membrane materials. One group with vanadium oxides was loaded to gas diffusion electrodes and tested ORR activity [24]. These compounds show an order of magnitude more current as cathode catalysts than anode catalysts therefore they may be viable candidates as cathode catalysts. Tungsten carbide has been tested as hydrogen oxidation catalyst. It is not stable enough under ORR conditions. Therefore, tantalum was added to WC to enhance

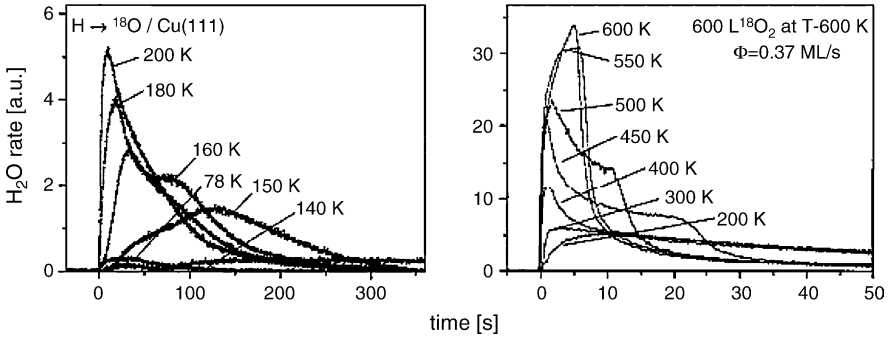

Fig. 10. Kinetics of water formation measured at various temperatures during admission of H to oxygen-covered Cu(1 1 1) surfaces (reproduced from [29] by permission of the American Chemical Society).

its potential electrocatalytic activity for ORR [25]. It was found that the corrosion resistance of the tungsten carbide is significantly increased by the addition of Ta to the pure WC catalyst. The electrocatalytic activity for the ORR in the WC + Ta catalyst was observed at 0.8 V, 0.35 V more positive than that of pure WC catalyst. Lanthanum manganite has been proposed as a catalyst for ORR [26]. The perovskite-type oxide was prepared through a reverse micelle assisted dispersion method. The products are fine particles, with size distribution around 3 nm. High cathodic performance above −0.15 V has been recorded under basic, room temperature conditions. The performance is comparable to Pt-loaded carbon electrode (0.56 mg cm^2). The ORR Catalytic activities of some selected metal compounds are compared in Table 1.

3. ORR catalyzed by organometallic complexes

A promising family of compounds, namely transition metal N_4-macrocycles such as porphyrin complexes, is known to catalyze oxygen reduction reaction under physiological conditions. These compounds have been extensively studied as the potential candidates as ORR catalysts for fuel cells because of their high catalytic activities. Other structurally similar transition metal complexes have been recently included in the hunt to find promising ORR catalysts. We will discuss the transition metal complexes according to the structures, starting from porphyrin-type compounds.

Table 1
Selected metal ORR catalysts

Catalyst	Preparation method	ORR activity	Reference
Pt		1.25 mA cm^{-2} at 0.51 V (vs. NHE)	[12]
Cu on Ru	Vacuum-deposition	Initial sticking efficient: 0.6 for 1 ML Cu, 0.002 for 3 ML Cu, 0.0005 for Cu	[3]
Au(1 1 1)	Sputtering	O_2 dissociation/ recombination at 77 K	[5]
Pd/Co (90:10)	H_2 reduction, 350 °C	65 nA at 0.6 V	[7]
$Mo_{4.2}Ru_{1.8}Se_8$	Thermolysis, 1500 °C	0.85 mA cm^{-2} at 0.51 V (vs. NHE)	[12]
WC + Ta	Sputtering	0.8 V (vs. DHE)	[22]
$LaMnO_{3+\delta}$	Reverse micelle assisted dispersion	0.3 A cm^2 at −80 mV (vs. Hg/HgO), 8 M KOH	[23]

3.1. Transition metal complexes with porphyrin ligands

The promising cathodic catalysts for fuel cell would reduce molecular oxygen through the direct four-electron process to water near the reversible thermodynamic potential (1.23 V versus NHE). In Section 1, oxygen adsorption on gold surfaces has been discussed. Modification of gold surface with metal complexes demonstrates significant influence on ORR activities. On the Au(1 1 1) surface, cobalt porphyrin complexes can form adlayers that enhance ORR activities on gold [27]. High-resolution STM images show uniformly formed Co–porphyrin complexes with clean molecular orientation on ordered domain (Fig. 11). Oxygen reduction on two types of cobalt–porphyrin complex modified gold electrodes both show enhanced activities (Fig. 12). There is obvious enhancement of reductive current for O_2 reduction at 0.32 V at the two modified electrodes. Compared to that of the bare Au surface, this current enhancement clearly shows that Co–porphyrin complex adlayer enhances ORR activity. Cytochrome *c* oxidase and related heme/copper terminal oxidases catalyze the complete four-proton, four-electron conversion of oxygen to water without releasing partially reduced peroxide intermediates that are toxic to cells. Metal complex systems similar to the enzymes thus possess promising potentials for ORR in fuel cells. Some enzyme catalyzed oxygen reduction reactions comprise proton-coupled electron-transfer process to facilitate the reaction. Attempts to mimic such process lead to the design of porphyrin platforms with precise control over the hydrogen-bonding functional nature [28]. The attachment of porphyrins to a rigid xanthene or dibenzofuran pillar bearing the H-bond pendant permits both the orientation and acid–base properties. The platforms with acid and ester hanging groups can orchestrate catalytic O–O bond activation and can yield superior catalysts to analogues that do not control both proton and

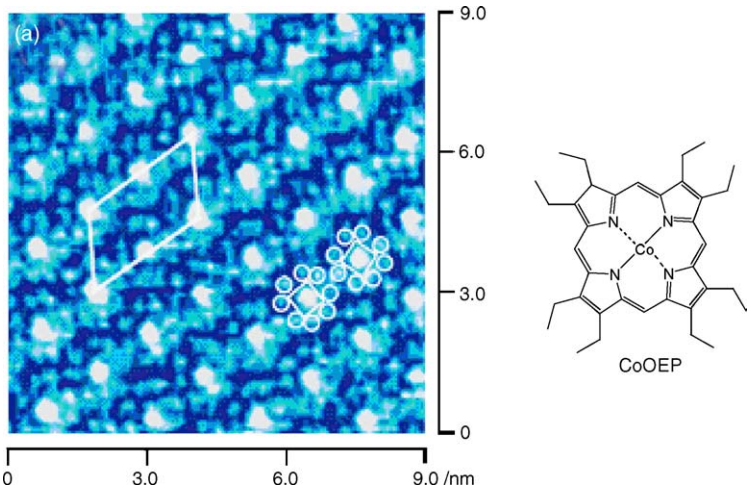

Fig. 11. High-resolution STM image shows the CoOEP adlayer formed on Au(1 1 1). Note the clear internal molecular structures and molecular orientations in the ordered domain (reproduced from [27] by permission of the American Chemical Society).

electron inventories. The reactivity studies for the disproportionation of hydrogen peroxide and the epoxidation of olefins by the platforms reveal that the introduction of a proton-transfer network can enhance O–O bond activation. Such proton-coupled ORR catalyzed by a family of dicobalt(II) cofacial bisporphyrins has also been investigated [29]. One compound reduces O_2 at a potential of 0.37 V with direct production of water at 80% selectivity (Fig. 13). In contrast, installation of a *trans*-aryl group (DPDM in Fig. 13) into this so-called Pacman motif results in decreased selectivity for the direct reduction of O_2 to water [30]. This selectivity decrease is attributed to subtle electronic and proton-coupled effects, not due to structural flexibility or redox behavior change. In the presence of similar cobalt complexes, the four-electron

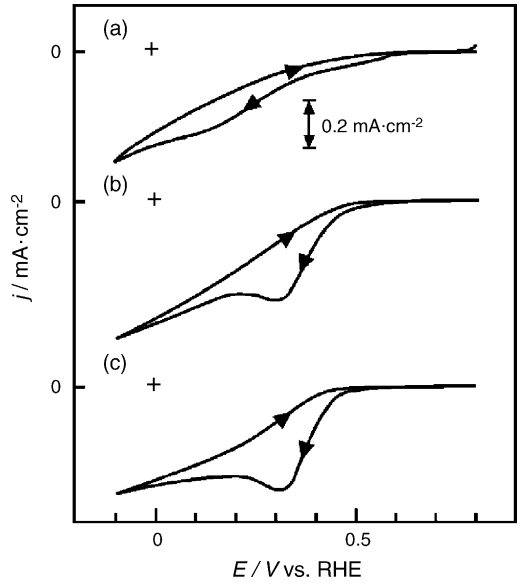

Fig. 12. CVs for the O_2 reduction at bare (a), CoP- (b), and CoOEP-modified (c) Au(1 1 1) electrodes in 0.1 M $HClO_4$ (reproduced from [27] by permission of the American Chemical Society).

reduction of O_2 by ferrocene derivatives as one-electron reducants was studied [31]. By monitoring the formation of the ferricenium ion, it was found that a cobalt porphyrin complex can reduce O_2 through a two-electron pathway with H_2O_2 as a product. With the dicobalt cofacial bisporphyrins, the concentration of the ferricenium ion is found to be four times the O_2 concentration, indicating a four-electron reduction. Catalytically active diiron(II)-μ-oxo complexes were synthesized from a tetraamidato macrocyclic Fe(III) complex [32]. These diiron complexes catalyze the selective oxidation of benzylic alcohols using molecular oxygen. It is hoped that some compounds with similar structures may possess ORR activity for fuel cells.

Beside the above discussed discrete porphyrin complexes, other metal complexes have been added to porphyrin systems to promote molecular oxygen reduction reactivity. A combination of porphyrin complexes and polyoxometallates was tested for ORR catalysis [33]. A 1:1 ratio of the two compounds in aqueous solution was adopted to form a supramolecular network, which was applied to a carbon RRDE. At −0.45 V, it was found that there are 3.8 electrons involved in the reduction of one O_2. Another study employs a molecular level-controlled assembly technique to form films of these two types of compounds on carbon electrode [34]. In the presence of O_2, a catalytic reduction current is observed at the electrode coated with multi-layer films (Fig. 14). The peak current of ORR is increased with more materials assembled onto the electrode. The peak potential of ORR is located at −0.18 V, a positive 0.5 V shift compared to non-modified carbon electrode. A ruthenium complex, $[Ru_3O(Ac)_6(py)_2]^+$ (Ac, acetate; py, pyridine) (Fig. 15), has been used to form supramolecular network with cobalt porphyrin [35]. CV curves of the complex show the redox processes of the three Ru from oxo-clusters. A carbon electrode modified with this complex demonstrates sharp and intense cathodic peaks around 0.2 V (Fig. 16). As shown in Fig. 16A, the current intensities, much more intense than the Ru(II/III)

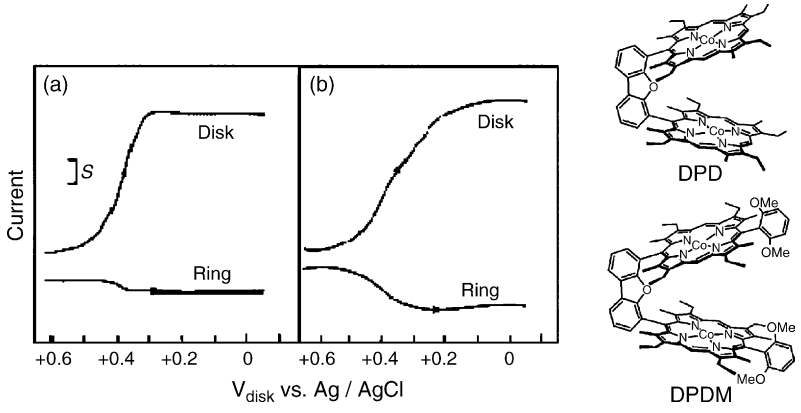

Fig. 13. Rotating Pt ring–disk voltammograms for reduction of O_2 at DPD-coated (a) and DPDM-coated (b) graphite disks. Disk current, $S = 10\,\mu A$; ring current, $S = 5\,\mu A$ (reproduced from [30] by permission of the American Chemical Society).

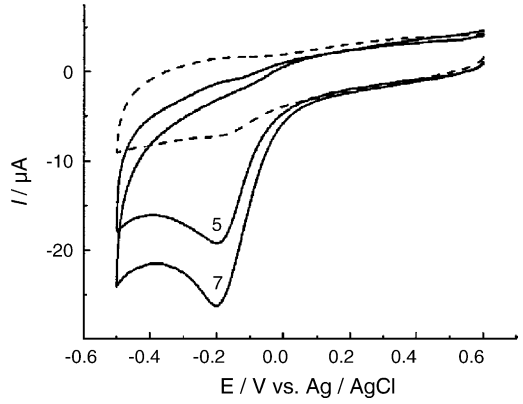

Fig. 14. CV of O_2 reduction at a carbon electrode coated with one cobalt porphyrin complex and one polyoxometallate. Dotted line: N_2-saturated solution (reproduced from [34] by permission of the American Chemical Society).

and Co(II/III) redox couples (Fig. 16B), vary as a linear function of the square root of the scan rate. More interestingly, the experimental results match perfectly the calculated peak currents for the four-electron ORR process (Fig. 16C). To illustrate the catalytic mechanism of such complexes, a molecular assembly technique was employed to prepare films containing this type of complexes [36]. From RRDE studies, the negligible ring currents and the slopes of the Levich and Koutecky–Levich plots approaching 4 are indicative of the theoretical four-electron ORR process. Because of the unique arrangement of the cobalt centers in the molecular assembled films, it is proved that the high catalytic activity of the supramolecular network is due to the activation of the cobalt porphyrin center by the coordination of the ruthenium clusters. A related study employs tetraruthenated cobalt–porphyrin and sulfonated zinc–porphyrin complexes to build assembly up to 50 bilayers [37]. The films exhibit very high conductivity when the potential approaches the redox potential of the Ru(II/III) couple. In another study, an iron(II) porphyrin was used as the ORR catalyst and $Ru(NH_3)_6^{2+}$ as the electron carrier in Nafion matrix [38]. When iron cobalt complex is directly adsorbed to the electrode, it behaves as a perfect four-electron ORR catalyst due to high availability of electrons. High $Ru(NH_3)_6^{2+}$ content favors such four-electron reaction catalyzed by the iron compound in Nafion matrix.

3.2. Transition metal complexes with non-porphyrin ligands

Common N_4-macrocycle ligands also include cyanine derivatives beside porphyrins. A cobalt phthalocyanine complex was found to catalyze ORR in alkaline solution [39]. Electron-withdrawing groups on cyanine are found to increase catalytic activity. In combination with manganese oxide, the same cobalt complex was found to catalyze a four-electron ORR in alkaline conditions [40]. This same complex was adsorbed onto Au(1 1 1) electrode surface and the ORR activity was analyzed [41]. The reduction current of O_2 commenced at ca. 0.45 V during the cathodic scan, a 0.15 V negative shift compared to bare Au(1 1 1) electrode. A clear electrocatalytic reduction peak of O_2 was found at ca. 0.2 V, indicating that the cobalt cyanine complex adlayer catalyzes the ORR (Fig. 17). At more negative potentials than 0.2 V, the reductive current remained almost constant because of the O_2 diffusion limitation. In contrast, a copper phthalocyanine complex does not show ORR activity.

Non-macrocycle, chelating ligands demonstrate similar coordination chemistry as the N_4-macrocycle members. Salen is a salicylideneamine compound and its vanadium complex is known to catalyze ORR [42]. Complexes of vanadium(III–V) with salen were examined to uncover the stoichiometry and kinetics of the reaction between O_2 and the V-salen complexes. In the presence of acid, oxygenation and disproportionation of $V^{III}(salen)^+$ provide the key catalysis for the four-electron ORR route. A series of Cu(I) complexes with tridentate animopyridine ligands was synthesized and structurally characterized [43]. The formation and subsequent reaction of O_2 with the complexes are observed (Scheme 2). Compared to complexes with a hydrogen or a methoxy group, the complex with a dimethyl amine group shows very high reactivity towards exogenous substrates such

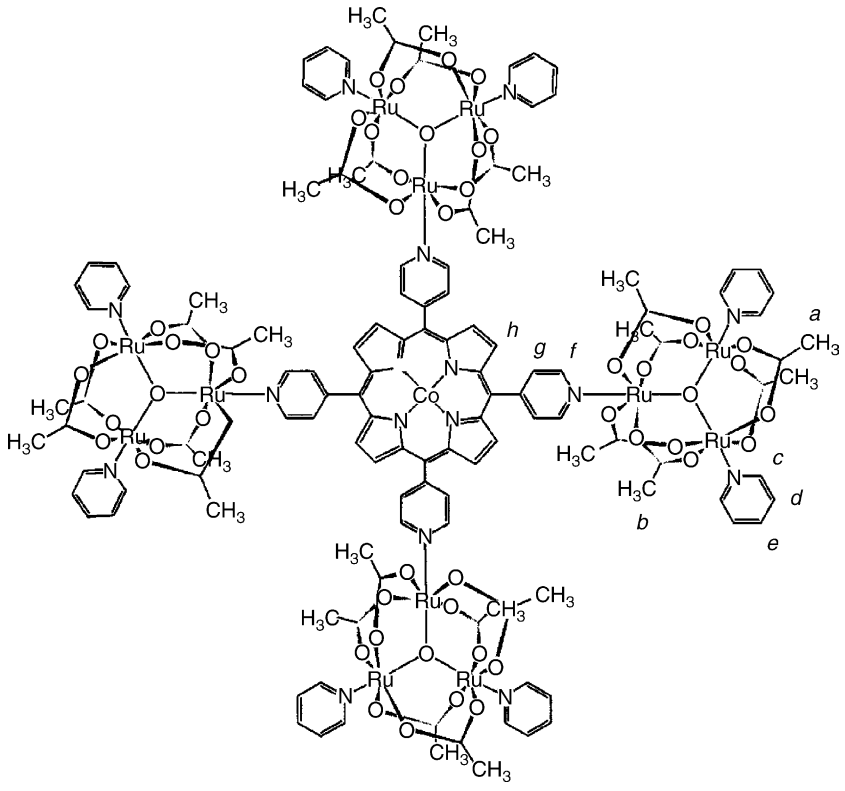

Fig. 15. Structure of 5,10,15,20-tetra(4-pyridyl)porphynato cobalt corrdinated to four $[\mu_3\text{-O-Ru}_3(Ac)_6(py)_2]^+$, CoTCP. Letters a–h indicate different protons in ^{1}H NMR (reproduced from [35] by permission of Elsevier).

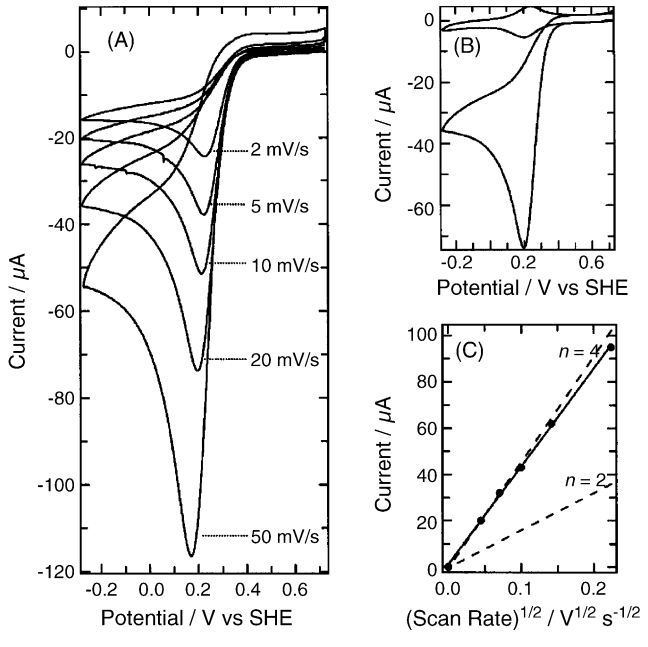

Fig. 16. (A) CV curves of the CoTCP-modified electrode in an air saturated solution at different scan rates. (B) Same as in (A), scan rate 20 mV s^{-1}, in the absence and presence of O_2. (C) Plot of the electrocatalytic O_2 reduction peak currents as a function of the square root of scan rates (solid circles and line) and the calculated curves for the reaction with $n = 2$ and $n = 4$ (dashed lines) (reproduced from [35] by permission of Elsevier).

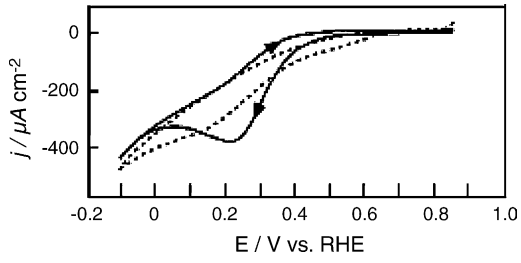

Fig. 17. Typical CV curves of bare (dotted) and cobalt phthalocyanine-adsorbed (solid) Au(1 1 1) electrodes in 0.1 M $HClO_4$ under O_2 (reproduced from [41] by permission of the American Chemical Society).

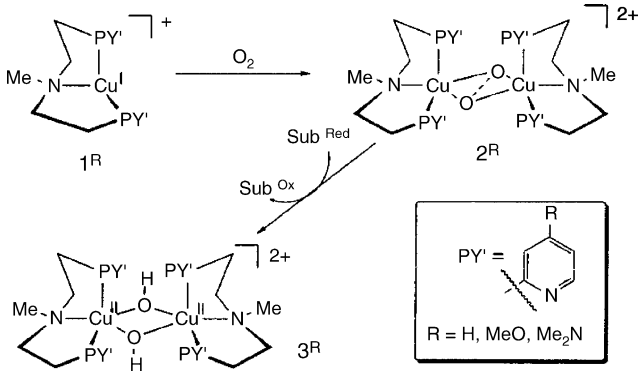

Scheme 2. (reproduced from [43] by permission of the American Chemical Society).

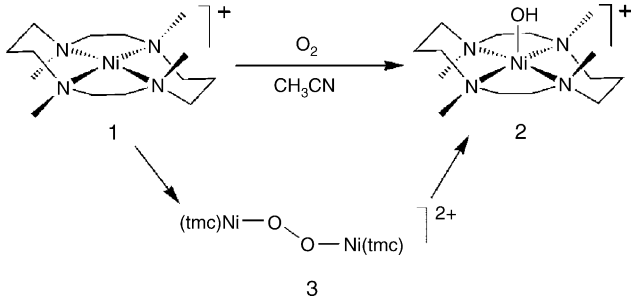

Scheme 3. (reproduced from [45] by permission of Wiley-VCH Verlag Gmbh & Co KG).

as THF. A different series of bis(μ-OH)diiron(II) complexes with polydentate animopyridine ligands has been synthesized and structurally characterized [44]. All four complexes react with O_2 in similar bimolecular associative processes. The complex with a tridentate ligand has fast oxygenation rate compared to those with tetradentate ligands. A nickel complex having a tetraazadodecane ligand was prepared and reacted with O_2 [45]. A binuclear μ-1,2-peroxo Ni_2 dimeric intermediate was characterized as the product of the oxygenation reaction at low temperature (Scheme 3). Thermal decomposition of this dimer leads to the formation of the hydroxy product.

Metal complexes of β-diketiminates are different from the abovementioned compounds in which the neutral N-donor ligands have been used. A set of Cu(I) β-diketiminate complexes were prepared with different backbone substituents that significantly impact the product oxygenation [46]. The complexes can be viewed as intermediates to form (superoxo)copper or bis(μ-oxo)dicopper species, which are of biological importance. Two 1:1 Cu–O_2 species have been isolated and the X-ray crystal structures been resolved. In Fig. 18, the oxygen molecule takes a side-on coordination with the copper atom in one such species [47,48]. These species can react with another copper(I) complex to form an asymmetric species (Fig. 19), which is very distinctive from other symmetric bis(μ-oxo) complexes.

Ligands that include elements other than nitrogen as the donor atoms have been employed to prepare complexes with ORR activity. A nickel(I) complex with thioether and borate donors was investigated [49]. For common nickel

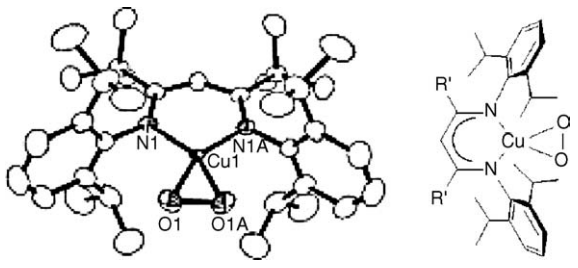

Fig. 18. X-ray crystal structure and chemical formula of one 1:1 Cu–O_2 species, showing all non-hydrogen atoms (reproduced from [47] by permission of the American Chemical Society).

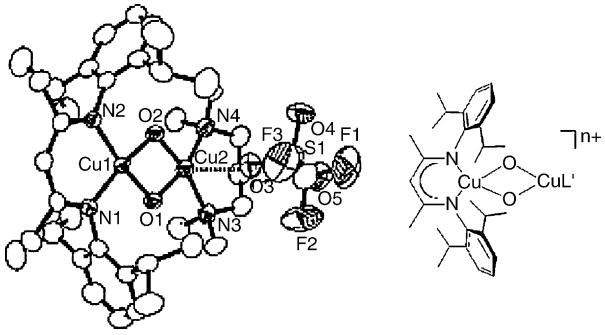

Fig. 19. X-ray crystal structure and chemical formula of one asymmetric bis(μ-oxo) species, showing all non-hydrogen atoms (reproduced from [47] by permission of the American Chemical Society).

thiolato complexes, oxygen sensitivity often causes disulfide formation. In this study, the borato ligand is able to support the nickel complexation with the thiolate ligands. This is also the first account of an $M_2(\mu\text{-}O_2)$ core supported by sulfur ligands. A similar complex reacts with O_2 generating a 1:1 species [50]. Based on the spectroscopic properties, this species is suggested as a side-on dioxygen adduct, a highly covalent Ni(II)–superoxo complex. A series of iron(II) α-keto carboxylate complexes have been prepared and reacted with dioxygen [51]. The oxygenation results in the hydroxylation of a phenyl position of the ligand to produce a phenolate product. The reaction mechanism is believed to involve dioxygen binding to form an iron(III) superoxide species with the oxidative decarboxylation of the adduct to afford the final product.

3.3. Heat-treated metal catalysts

For the N_4-macrocycle (such as porphyrin) metal complexes, the formation of H_2O_2 is believed to be responsible for the deterioration of electrode performance over time. Heat-treatment of such complexes is found to overcome these shortcomings. On the carbon-supported, pyrolyzed iron(III) tetramethoxyphenyl porphyrin chloride, it is possible to reduce H_2O_2 electrochemically [52]. The number of electrons exchanged per O_2 is between 3.45 and 4 in the heat-treatment temperature range of 400–000 °C (Fig. 20). The O_2 reduction is postulated to comprise both direct and series reaction paths. The increased catalytic activity by the heat-treatment is likely caused by the decrease in the activation energy of the reaction. The active site of O_2 reduction on pyrolyzed carbon-supported iron porphyrin catalysts was studied via ex situ and in situ ^{57}Fe Mössbauer spectrometry [53]. In combination with X-ray absorption spectroscopy and X-ray photoelectron spectroscopy, the Fe–N_4 moiety was found to be the site of the O_2 reduction activity even after a heat treatment up to 800 °C. The enhanced ORR activity of such heat-treated M–N_4 species is likely due to a higher number of active Fe^{2+} sites at oxygen reduction potentials. The M–N_4 moiety does retain after heat-treatment at temperature as high as 800 °C, and the core is the catalytic site.

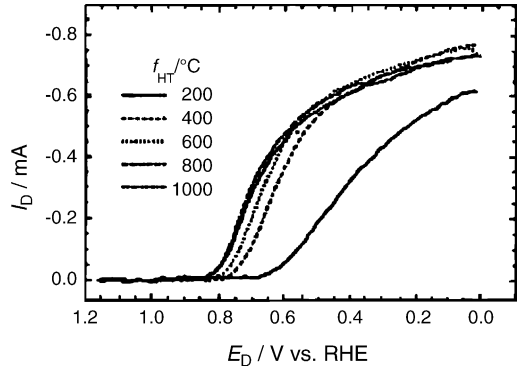

Fig. 20. Disk currents for O_2 reduction on heat-treated iron porphyrin complex (reproduced from [52] by permission of Elsevier).

Dodelet and coworkers used a modified procedure to provide better control over metal impurities during heat-treatment [54]. Their procedure uses perylene tetracarboxylic dianhydride, free of metal impurities, as a precursor for the carbon support. Iron porphyrin complex was mixed with this material followed by pyrolysis at various temperatures. A $FeN_2C_4^+$ moiety was found by secondary ion mass spectrometry (SIMS) to be the catalytic site at pyrolysis temperature above 800 °C. A 2% iron content was found to be most promising for ORR catalysis. Because the FeN_2C_y moiety is found to be the active catalytic site for ORR, non-porphyrin iron complexes have been employed in the heat-treatment process in the same study. Iron(II) acetate was pyrolyzed in the presence of NH_3 to afford such active moieties. A 0.2% iron acetate content provides the most performing catalyst. A later study by using SIMS in combination with catalytic activity revealed that there are more than one active species [55]. It was found that two different catalytic sites exist simultaneously in all catalysts. FeN_4/C represents one family of ions ($FeN_4C_y^+$, $FeN_3C_y^+$, and $FeNC_y^+$) and the other group has FeN_2/C as the core, whose most representative ion is $FeN_2C_4^+$. FeN_2/C group is more electrocatalytically active than FeN_4/C group. Compared to the iron porphyrin complex precursor method, the preparation method with iron acetate plus ammonia as precursors can yield a catalyst that is 80% of the more active FeN_2/C sites. The method of using iron acetate as precursor for heat-treatment was later explored with various carbon supports [56]. The activity of the catalysts varies greatly from one carbon support to another, but neither the specific surface area of the catalysts nor the distribution of their macro- or meso-pores seems to be a determining factor for the catalytic activity. The most important factor is the N content of the materials; the higher it is, the higher is the density of the catalytic sites on their surface and the better is the electrocatalyst (Fig. 21). In the materials examined, three catalytic sites are at work: FeO/C, FeN_4/C and FeN_2/C, with the last site being the most active for ORR. It was further confirmed that catalysts prepared with the same carbon support demonstrate different catalytic activities depending upon the treatment applied to the chosen support [57]. A best procedure is described as pretreating

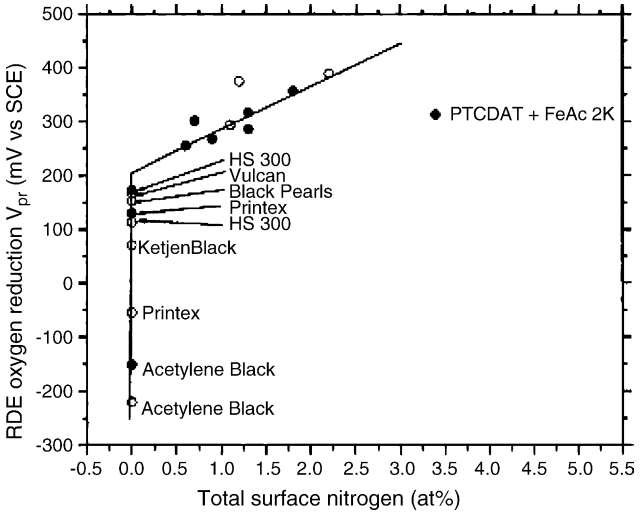

Fig. 21. Change in catalytic activity with total nitrogen concentration of the catalysts from XPS results. Open circles: non-treated carbon supports. Solid circles: treated carbon supports (reproduced from [56] by permission of the American Chemical Society).

the carbon support with HNO_3, followed by adsorbing iron acetate on the support, then by a last heat-treatment of the resulting material at 900 °C in NH_3. This procedure provides the nitrogen enrichment of the carbon supports, which in turn may increase the interaction of iron acetate with the carbon support and results in a better molecular dispersion of iron on the surface.

Other metal complexes have been conducted heat-treatment. Pyrolysis of iron phthalocyanine on nickel substrates can produce carbon nanofiber electrodes existing in aligned bundles [58]. These electrodes demonstrate significant electrocatalytic activity in aqueous KNO_3 solutions at neutral to basic pH for the reduction of O_2 to HO_2^-. This peroxide pathway via two successive two-electron reductions has been verified through electrochemical methods. It is suggested that the disorder in the graphite fibers and the presence of exposed edge plane defects and nitrogen moieties are important factors for enhancing electrocatalysis for ORR. Likewise, heat-treatment was applied to transition metal cyanide complexes to provide ORR catalysts [59]. A combination of cobalt and iron incorporated at neighboring sites produces the highest activity, comparable to platinum black catalyst (Pt/C). More promising is that the ORR catalytic activity is not affected by the presence of 2.5 M methanol, in stark contrast to the performance of Pt/C (Fig. 22). XRD and XPS data indicate the decomposition of cyanide structure when heating beyond 500 °C, and two types of nitrogen forming new bonding are present in the samples.

4. Development of ORR catalyst assemblies

There is a recent review on electrode design for PEMFC [60] that provides a detailed description of general consid-

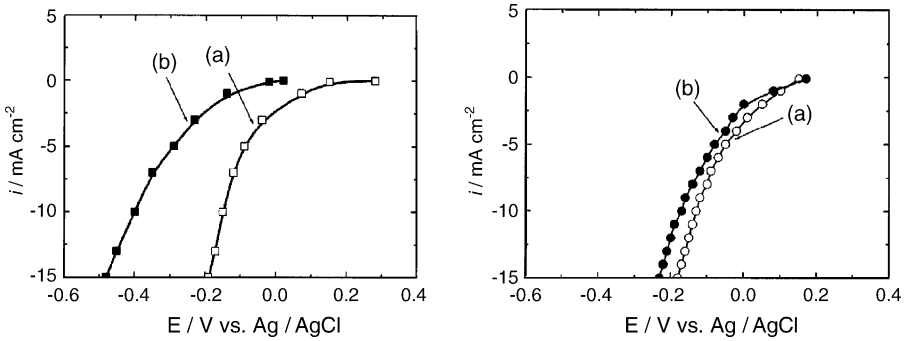

Fig. 22. Polarization curves for ORR with (left) Pt/C and (right) heat-treated cobalt/iron cyanine complex in the (a) absence and (b) presence of 2.5 M methanol in the electrolyte under air (reproduced from [59] by permission of the Electrochemical Society, Inc.).

erations for electrodes. Here, some specific features for the design of the cathodic electrode are discussed. The above-mentioned catalysts are either metal slabs that can be directly used as the electrode, or metal-containing compounds that are applied as coatings onto electrode surfaces. Recent advancements in materials fabrication techniques applying nanotechnology have provided new frontiers in the development of ORR catalysts. As discussed in Section 2, nano-scale metal oxides have been used for ORR. However, many metal oxides dissolve under the very acidic PEMFC working conditions. Conducting polymer polypyrrole (PPy) layers were used to protect against the dissolution of metal oxide $Ni_{0.3}Co_{2.7}O_4$ [61]. Both the oxide and PPy were electrodeposited onto carbon electrodes in such a fashion that the oxide is sandwiched between PPy layers. A remarkable electrochemical stability of the oxide at acidic condition is achieved. Also impressing is the observation that the retaining of electrical conductivity of the composite film at potentials at which PPy is usually in an insulator state. Continuation of research in such systems extends to the effect of the counter ions in the composite [62]. It is believed that electrical conductivity is directly related to the electropolymerization processes. Counter anions have a profound effect on the polymerization process and the resulting composites demonstrate characteristic ORR activities (Fig. 23). A similar study utilized $CoFe_2O_4$ and PPy to form sandwiched composites [63]. The electrode exhibits high electrocatalytic reactivity towards oxygen reduction and stability in acidic media and high cathodic potential conditions. Metal oxide nanoparticles embedded in a conductive polymer matrix seems a promising design for ORR electrode. Poly(vinylpyridine) (PVP) confined iron(III) cyanide shows surprisingly catalytic activity for H_2O_2 reduction that is absent when $Fe(CN)_6^{3-}$ is in solution phase [64]. The reason for this catalytic activity is ascribed to the coordination of iron to pyridine molecules in the polymer, which forms an open coordination site in the $Fe(CN)_6^{3-}$ complex. Leaching of Fe from the PVP leads to loss of the catalytic activity. Electrodeposition of small Au particles has proven to stabilize the iron catalyst in the PVP films.

Although this article concentrates on non-Pt catalysts, some electrode designs using Pt may be modified for non-Pt systems. Conventional activated carbon loaded with dispersed Pt has been used as the staple catalyst as a highly active catalyst for ORR. However, slow transfer of oxygen and proton in the pores hinders the electrode reaction. Triflic acid, CF_3SO_2H, was added into the pores of activated carbon to increase the proton transfer and O_2 diffusion [65]. The activity of the catalyst layer composed of dispersed Pt in such carbon substrate has increased ca. eight-fold when compared to the results from systems with conventional carbon substrate. Electrode potential of 0.1–0.15 V improvements can be attained. Gas diffusion electrodes are used in most PEMFC designs. The diffusion layer provides a physical micro porous base through its channels reactants reach the catalyst layer. A hydrophobic carbon layer immobilized in the gas diffusion electrode has been studied [66]. The electrode assembly with

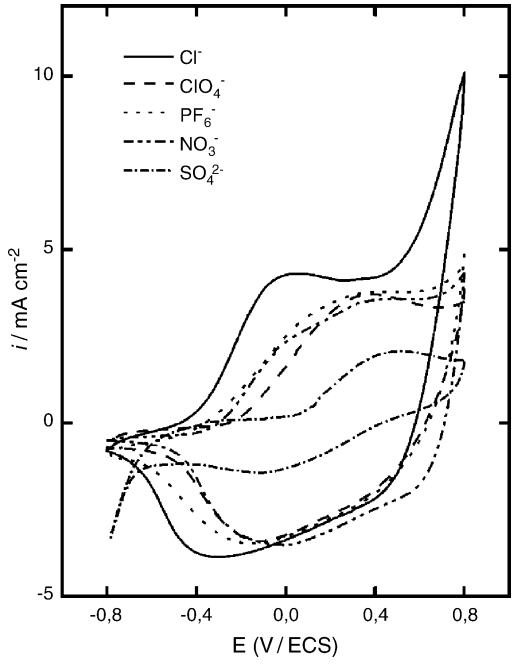

Fig. 23. CV curves of an electrode made of $Cu_{1.4}Mn_{1.6}O_4$ inside PPy matrix, doped with various anions, pH 2.2 (reproduced from [62] by permission of Elsevier).

such a diffusion layer demonstrates high efficiencies at high current densities, yet the assembly without such a layer performs better at low current densities. No explanation of the mechanism involved is given in the article.

5. Outlook for ORR catalyst development

Both materials chemistry and engineering have improved significantly over the past decade or so in the ORR catalyst area. Future development may lead to highly efficient and economical catalysts with these features: non-Pt containing, nanoparticle-based, molecular-level assemblies. The nanometer scale distribution of catalyst centers on electrode surface seems to be a predominant factor for high catalytic activities. This fact requires the employment of nanoparticulate materials as the catalysts. When such small-size thus small-mass materials are used as the electrode catalysts, the seemingly cost difference between some very inexpensive metals (i.e., Cu, Fe) and some relatively more expensive ones (i.e., Au, Ag) becomes less significant. Therefore, any selection of catalyst materials will depend more so on performance and processing cost. Platinum is precluded here because of its scarcity, not just because of its cost. The most efficient fabrication of nanoparticle catalyst is through molecular-level assembly. The combination of molecular-level assembly and other assisting techniques such as heat-treatment may afford significantly effective systems for ORR catalysis.

References

[1] For a general review of fuel cell vehicle technology, please visit Fuel Economy Agency Website at www.fueleconomy.gov.

[2] J. Prakash, H. Joachin, Electrocatalytic activity of ruthenium for oxygen reduction in alkaline solution, Electrochim. Acta 45 (2000) 2289–2296.

[3] R. Otero, F. Calleja, V.M. García-Suárez, J.J. Hinarejos, J. de la Figuera, J. Ferrer, A.L. Vázquez de Parga, R. Miranda, Tailoring surface electronic states via strain to control adsorption: O/Cu/Ru(0 0 0 1), Surf. Sci. 550 (2004) 65–72.

[4] Y. Xu, M. Mavrikakis, Adsorption and dissociation of O_2 on gold surfaces: effect of steps and strain, J. Phys. Chem. B 107 (2003) 9298–9307.

[5] J.D. Stiehl, T.S. Kim, S.M. McClure, C.B. Mullins, Evidence for molecularly chemisorbed oxygen on TiO_2 supported gold nanoclusters and Au(1 1 1), J. Am. Chem. Soc. 126 (2004) 1606–1607.

[6] J.D. Stiehl, T.S. Kim, S.M. McClure, C.B. Mullins, Formation of molecularly chemisorbed oxygen on TiO2-supported gold nanoclusters and Au(1 1 1) from exposure to an oxygen plasma jet, J. Phys. Chem. B 109 (2005) 6316–6322.

[7] S.B. Aoun, Z. Dursun, T. Sotomura, I. Taniguchi, Effect of metal adlayers on Au(1 1 1) electrodes on electrocatalytic reduction of oxygen in an alkaline solution, Electrochem. Commun. 6 (2004) 747–752.

[8] J.L. Fernández, D.A. Walsh, A.J. Bard, Thermodynamic guidelines for the design of bimetallic catalysts for oxygen electroreduction and rapid screening by scanning electrochemical microscopy. M–Co (M:Pd, Ag, Au), J. Am. Chem. Soc. 127 (2005) 357–365.

[9] M.S. El-Deab, T. Sotomura, T. Ohsaka, Oxygen reduction at electrochemically deposited crystallographically oriented Au(1 0 0)-like gold nanoparticles, Electrochem. Commun. 7 (2005) 29–34.

[10] W.T. Wallace, R.B. Wyrwas, R.L. Whetten, R. Mitrić, V. Bonačić-Koutecký, Oxygen adsorption on hydrated gold cluster anions: experiment and theory, J. Am. Chem. Soc. 125 (2003) 8408–8414.

[11] I. Yagi, T. Ishida, K. Uosaki, Electrocatalytic reduction of oxygen to water at Au nanoclusters vacuum-evaporated on boron-doped diamond in acidic solution, Electrochem. Commun. 6 (2004) 773–779.

[12] Y. Shen, L. Bi, B. Liu, S. Dong, Simple preparation method of Pd nanoparticles on an Au electrode and its catalysis for dioxygen reduction, New J. Chem. 27 (2003) 938–941.

[13] Y. Lin, X. Cui, X. Ye, Electrocatalytic reactivity for oxygen reduction of palladium-modified carbon nanotubes synthesized in supercritical fluid, Electrochem. Commun. 7 (2005) 267–274.

[14] L. Demarconnay, C. Coutanceau, J.M. Léger, Electroreduction of dioxygen (ORR) in alkaline medium on Ag/C and Pt/C nanostructured catalysts-effect of the presence of methanol, Electrochim. Acta 49 (2004) 4513–4521.

[15] N.A. Vante, H. Tributsch, Energy conversion catalysis using semiconducting transition metal cluster compounds, Nature 323 (1986) 431–432.

[16] H. Tributsch, M. Bron, M. Hilgendorff, H. Schulenburg, I. Dorbandt, V. Eyert, P. Bogdanoff, S. Fiechter, Methanol-resistant cathodic oxygen reduction catalysts for methanol fuel cells, J. Appl. Electrochem. 31 (2001) 739–748.

[17] X. Chen, G. Chen, Stable Ti/RuO_2–Sb_2O_5–SnO_2 electrodes for O_2 evolution, Electrochim. Acta 50 (2005) 4155–4159.

[18] S. Ohno, K. Yagyuu, K. Nakatsuji, F. Komori, Dissociation preference of oxygen molecules on an inhomogeneously strained Cu(0 0 1) surface, Surf. Sci. 554 (2004) 183–192.

[19] Th. Kammler, J. Küppers, The kinetics of the reaction of gaseous hydrogen atoms with oxygen on Cu(1 1 1) surfaces toward water, J. Phys. Chem. B 105 (2001) 8369–8374.

[20] D. Kolovos-Vellianitis, Th. Kammler, J. Küppers, Interaction of gaseous hydrogen atoms with oxygen covered Cu(1 0 0) surfaces, Surf. Sci. 482–485 (2001) 166–170.

[21] D. Kolovos-Vellianitis, J. Küppers, Kinetics of abstraction of D and O on Cu(1 1 0) surfaces by gaseous H atoms, J. Phys. Chem. B 107 (2003) 2559–2564.

[22] B. Lescop, J.Ph. Jay, G. Fanjoux, Reduction of oxygen pre-treated Ni(1 1 1) by H_2 exposure: UPS and MIES studies compared with Monte Carlo simulations, Surf. Sci. 548 (2004) 83–94.

[23] S.V. Mentus, Oxygen reduction on anodically formed titanium dioxide, Electrochim. Acta 50 (2004) 27–32.

[24] B.R. Limoges, R.J. Stanis, J.A. Turner, A.M. Herring, Electrocatalyst materials for fuel cells based on the polyoxometalates $[Pmo_{(12-n)}V_nO_{40}]^{(3+n)-}$ ($n = 0$–3), Electrochim. Acta 50 (2005) 1169–1179.

[25] K. Lee, A. Ishihara, S. Mitsushima, N. Kamiya, K. Ota, Stability and electrocatalytic activity for oxygen reduction in WC + Ta catalyst, Electrochim. Acta 49 (2004) 3479–3485.

[26] M. Hayashi, H. Uemura, K. Shimanoe, N. Miura, N. Yamazoe, Reverse micelle assisted dispersion of lanthanum manganite on carbon support for oxygen reduction cathode, J. Electrochem. Soc. 151 (2004) A158–A163.

[27] S. Yoshimoto, J. Inukai, A. Tada, T. Abe, T. Morimoto, A. Osuka, H. Furuta, K. Itaya, Adlayer structure of and electrochemical O_2 reduction on cobalt porphine-modified and cobalt octaethylporphyrin-modified Au(1 1 1) in $HClO_4$, J. Phys. Chem. B 108 (2004) 1948–1954.

[28] C.J. Chang, L.L. Chng, D.G. Nocera, Proton-coupled O–O activation on a redox platform bearing a hydrogen-bonding scaffold, J. Am. Chem. Soc. 125 (2003) 1866–1876.

[29] C.J. Chang, Y. Deng, C. Shi, C.K. Chang, F.C. Anson, D.G. Nocera, Electrocatalytic four-electron reduction of oxygen to water by a

highly flexible cofacial cobalt bisporphyrin, Chem. Commun. (2000) 1355–1356.
[30] C.J. Chang, Z.-H. Loh, C. Shi, F.C. Anson, D.G. Nocera, Targeted proton delivery in the catalyzed reduction of oxygen to water by bimetallic Pacman porphyrins, J. Am. Chem. Soc. 126 (2004) 10013–10020.
[31] S. Fukuzumi, K. Okamoto, C.P. Gros, R. Guilard, Mechanism of four-electron reduction of dioxygen to water by ferrocene derivatives in the presence of perchloric acid in benzonitrile, catalyzed by cofacial dicobalt poyphyrins, J. Am. Chem. Soc. 126 (2004) 10441–10449.
[32] A. Ghosh, F.T. de Oliveira, T. Yano, T. Nishioka, E.S. Beach, I. Kinoshita, E. Münck, A.D. Ryabov, C.P. Horwitz, T.J. Collins, Catalytically active μ-oxodiiron(IV) oxidants from iron(III) and dioxygen, J. Am. Chem. Soc. 127 (2005) 2505–2513.
[33] S.-Q. Liu, J.-Q. Xu, H.-R. Sun, D.-M. Li, *meso*-Tetrakis(4-*N*-benzylpyridyl)-porphyrin and its supramolecular complexes formed with anionic metal-oxo cluster: spectroscopy and electrocatalytic reduction of dioxygen, Inorg. Chim. Acta 306 (2000) 87–93.
[34] Y. Shen, J. Liu, J. Jiang, B. Liu, S. Dong, Fabrication of a metallopoyphyrin-polyoxometalate hybrid film by a layer-by-layer method and its catalysis for hydrogen evolution and dioxygen reduction, J. Phys. Chem. B 107 (2003) 9744–9748.
[35] K. Araki, S. Dovidauskas, H. Winnischofer, A.D.P. Alexiou, H.E. Toma, A new highly efficient tetra-electronic catalyst based on a cobalt porphyrin bound to four μ_3-oxo-ruthenium acetate clusters, J. Electroanal. Chem. 498 (2001) 152–160.
[36] H. Winnischofer, V.Y. Otake, S. Dovidauskas, M. Nakanura, H.E. Toma, K. Araki, Supramolecular tetracluster-cobalt porphyrin: a four-electron transfer catalyst for dioxygen reduction, Electrochim. Acta 49 (2004) 3711–3718.
[37] J.R.C. da Rocha, G.J.F. Demets, M. Bertotti, K. Araki, H.E. Toma, Charge transfer at electrostatically assembled tetraruthenated porphyrin modified electrodes, J. Electroanal. Chem. 526 (2002) 69–76.
[38] J.P. Collman, I.M. Shiryaeva, R. Boulatov, Effect of electron availability on selectivity of O_2 reduction by synthetic monometallic Fe porphyrins, Inorg. Chem. 42 (2003) 4807–4809.
[39] G.I. Cárdenas-Jirón, M.A. Gulppi, C.A. Caro, R. del Río, M. Páez, J.H. Zagal, Reactivity of electrodes modified with substituted metallophthalocyanines. Correlations with redox potentials, Hammett parameters and donor–acceptor intermolecular hardness, Electrochim. Acta 46 (2001) 3227–3235.
[40] K. Arihara, L. Mao, P.A. Liddell, E. Marino-Ochoa, A.L. Moore, T. Imase, D. Zhang, T. Sotomura, T. Ohsaka, Electrocatalytic reduction of oxygen in a novel catalytic system with cobalt phthalocyanines and manganese oxide, J. Electrochem. Soc. 151 (2004) A2047–A2052.
[41] S. Yoshimoto, A. Tada, K. Suto, K. Itaya, Adlayer structures and electrocatalytic activity for O_2 of metallophthalocyanines on Au(1 1 1): in situ scanning tunnelling microscopy study, J. Phys. Chem. B 107 (2003) 5836–5843.
[42] Z. Liu, F.C. Anson, Electrochemical properties of vanadium(III, IV, V)–salen complexes in acetonitrile. Four-electron reduction of O_2 by V(III)–salen, Inorg. Chem. 39 (2000) 274–280.
[43] C.X. Zhang, H.-C. Liang, E. Kim, J. Shearer, M.E. Helton, E. Kim, S. Kaderli, C.D. Incarvito, A.D. Zuberbühler, A.L. Rheingold, K.D. Karlin, Tuning copper-dioxygen reactivity and exogenous substrate oxidations via alterations in ligand electronics, J. Am. Chem. Soc. 125 (2003) 634–635.
[44] S.V. Kryatov, S. Taktak, I.V. Korendovych, E.V. Rybak-Alimova, J. Kaizer, S. Torelli, X. Shan, S. Mandal, V.L. MacMurdo, A.N. i Payeras, L. Que Jr., Dioxygen binding to complexes with $Fe(II)_2(\mu\text{-}OH)_2$ cores: steric control of activation barriers and O_2-adduct formation, Inorg. Chem. 44 (2005) 85–99.
[45] M.T. Kieber-Emmons, R. Schenker, G.P.A. Yap, T.C. Brunold, C.G. Riordan, Spectroscopic elucidation of a peroxo $Ni_2(\mu\text{-}O_2)$ intermediate derived from a nickel(I) complex and dioxygen, Angew. Chem. Int. Ed. 43 (2004) 6716–6718.
[46] D.J.E. Spencer, N.W. Aboelella, A.M. Reynolds, P.L. Holland, W.B. Tolman, β-Ditetiminate ligand backbone structural effects on $Cu(I)/O_2$ reactivity: unique copper–superoxo and bis(μ-oxo) complexes, J. Am. Chem. Soc. 124 (2002) 2108–2109.
[47] N.W. Aboelella, E.A. Lewis, A.M. Reynolds, W.W. Brennessel, C.J. Cramer, W.B. Tolman, Snapshots of dioxygen activation by copper: the structure of a 1:1 Cu/O_2 adduct and its use in syntheses of asymmetric bis(μ-oxo) complexes, J. Am. Chem. Soc. 124 (2002) 10660–10661.
[48] N.W. Aboelella, S.V. Kryatov, B.F. Gherman, W.W. Brennessel, V.G. Young Jr., R. Sarangi, E.V. Rybak-Akimova, K.O. Hodgson, B. Hedman, E.I. Solomon, C.J. Cramer, W.B. Tolman, Dioxygen activation at a single copper site: structure, bonding, and mechanism of formation of 1:1 $Cu–O_2$ adducts, J. Am. Chem. Soc. 126 (2004) 16896–16911.
[49] B.S. Mandimutsira, J.L. Yamarik, T.C. Brunold, W. Gu, S.P. Cramer, C.G. Riordan, Dioxygen activation by a nickel thioether complex: characterization of a $Ni(III)_2(\mu\text{-}O)_2$ core, J. Am. Chem. Soc. 123 (2001) 9194–9195.
[50] K. Fujita, R. Schenker, W. Gu, T.C. Brunold, S.P. Cramer, C.G. Riordan, A monomeric nickel-dioxygen adduct derived from a nickel(I) complex and O_2, Inorg. Chem. 43 (2004) 3324–3326.
[51] M.P. Mehn, K. Fujisawa, E.L. Hegg, L. Que Jr., Oxygen activation by nonheme iron(II) complexes: α-keto carboxylate versus carboxylate, J. Am. Chem. Soc. 125 (2003) 7828–7842.
[52] S.Lj. Gojković, S. Gupta, R.F. Savinell, Heat-treated iron(III) tetramethoxyphenyl porphyrin chloride supported on high-area carbon as an electrocatalyst for oxygen reduction: part 3, detection of hydrogen-peroxide during oxygen reduction, Electrochim. Acta 45 (1999) 889–897.
[53] A.L. Bouwkamp-Wijnoltz, W. Visscher, J.A.R. van Veen, E. Boellaard, A.M. van der Kraan, On active-site heterogeneity in pyrolyzed carbon-supported iron poyphyrin catalysts for the electrochemical reduction of oxygen: an in situ Mössbauer study, J. Phys. Chem. B 106 (2002) 12993–13001.
[54] M. Lefèvre, J.P. Dodelet, P. Bertrand, O_2 reduction in PEM fuel cells: activity and active site structural information for catalysts obtained by the pyrolysis at high temperature of Fe precursors, J. Phys. Chem. B 104 (2000) 11238–11247.
[55] M. Lefèvre, J.P. Dodelet, P. Bertrand, Molecular oxygen reduction in PEM fuel cells: evidence for the simultaneous presence of two active sites in Fe-based catalysts, J. Phys. Chem. B 106 (2002) 8705–8713.
[56] F. Jaouen, S. Marcotte, J.P. Dodelet, G. Lindbergh, Oxygen reduction catalysts for polymer electrolyte fuel cells from the pyrolysis of iron acetate adsorbed on various carbon supports, J. Phys. Chem. B 107 (2003) 1376–1386.
[57] D. Villers, X. Jacques-Bédard, J.P. Dodelet, Fe-based catalysts for oxygen reduction in PEM fuel cells, pre-treatment of the carbon support, J. Electrochem. Soc. 151 (2004) A1507–A1515.
[58] S. Maldonado, K.J. Stevenson, Direct preparation of carbon nanofiber electrodes via pyrolysis of iron(II) phthalocyanine: electrocatalytic aspects for oxygen reduction, J. Phys. Chem. B 108 (2004) 11375–11383.
[59] K. Sawai, N. Suzuki, Heat-treated transition metal hexacyanometallates as electrocatalysts for oxygen reduction insensitive to methanol, J. Electrochem. Soc. 151 (2004) A682–A688.
[60] S. Ltster, G. MLean, PEM fuel cell electrodes, J. Power Sources 130 (2004) 61–76.
[61] J.L. Gautier, J.F. Marco, M. Gracia, J.R. Gancedo, V. de la Garza Guadarrama, H. Nguyen-Cong, P. Chartier, $Ni_{0.3}Co_{2.7}O_4$ spinel particles/polypyrrole composite electrode: study by X-ray photoelectron spectroscopy, Electrochim. Acta 48 (2002) 119–125.
[62] H. Nguyen-Cong, K. El Abbassi, J.L. Gautier, P. Chartier, Oxygen reduction on oxide/polypyrrole composite electrode: effect of doping anions, Electrochim. Acta 50 (2005) 1369–1376.

[63] R.N. Singh, B. Lal, M. Malviya, Electrocatalytic activity of electrodeposited composite films of polypyrrole and $CoFe_2O_4$ nanoparticles towards oxygen reduction reaction, Electrochim. Acta 49 (2004) 4605–4612.
[64] J. Kim, A.A. Gewirth, Electrocatalysis of peroxide reduction by Au-stabilized, Fe-containing poly(vinylpyridine) films, J. Phys. Chem. B 109 (2005) 9684–9690.
[65] J. Maruyama, I. Abe, Effective utilization of nanospaces in activated carbon for enhancing catalytic activity in fuel cell electrodes, J. Electrochem. Soc. 151 (2004) A47–A451.
[66] J. Mirzazadeh, E. Saievar-Iranizad, L. Nahavandi, An analytical approach on effect of diffusion layer on ORR for PEMFCs, J. Power Sources 131 (2004) 194–199.